

Formation Mechanism of $120^\circ\langle 111 \rangle$ Twin Boundaries in γ Phase of a TiAl Based Alloy During Annealing Treatment in Hydrogen Atmosphere

Wen Daosheng¹, Wang Shouren¹, Shan Debin², Zong Yingying²

¹ University of Jinan, Jinan 250022, China; ² State Key Laboratory of Advanced Welding and Joining, Harbin Institute of Technology, Harbin 150001, China

Abstract: The effect of hydrogen on $120^\circ\langle 111 \rangle$ twin boundaries in γ phase of as-cast and as-forged Ti-46Al-2V-1Cr-0.3Ni alloys was investigated by annealing treatment in hydrogen atmosphere, and the microstructure was observed by an optical microscope, a scanning electron microscope, an electron back scattered diffraction technique, a transmission electron microscope and a X-ray diffraction apparatus. The results show that hydrogen could promote γ -phase static recrystallization of the as-cast and as-forged alloys, and the extent of static recrystallization increases with increasing the hydrogen content. Many static recrystallization grains possess $120^\circ\langle 111 \rangle$ twin boundaries. The relationship between the fraction of $120^\circ\langle 111 \rangle$ twin boundaries and hydrogen content is given. Hydrogen-weakened γ -phase elastic anisotropy increases $120^\circ\langle 111 \rangle$ twin boundaries.

Key words: TiAl based alloy; annealing treatment; hydrogen; static recrystallization; $120^\circ\langle 111 \rangle$ twin boundaries

Although TiAl based alloys have increasingly attracted attention due to their noticeable engineering application prospect in aviation and aerospace^[1-3], while such application is restricted by poor ductility and fracture toughness^[4]. γ phase is generally dominant in TiAl based alloys and so has critical effect on mechanical properties. In γ phase, three types of twins, namely pseudo ($60^\circ\langle 111 \rangle$), true ($180^\circ\langle 111 \rangle$) and order ($120^\circ\langle 111 \rangle$) twins, have been distinguished^[5]. Twins can occur during annealing or deformation, and consequently form annealing twin boundaries and deformation twin boundaries^[6-9]. Annealing twin boundaries have important influence on the mechanical properties, such as stronger resistance to intergranular degradation than the random boundaries^[10-12]. Since 'grain boundary design' was proposed^[13], quantities of works have been conducted on grain boundary engineering (GBE) to improve GBE-related properties^[14-19].

Previous works report that many GBE-related findings are

obtained in austenitic stainless steel^[11], Ni-based alloys^[15,16], copper and its alloys^[17]. By means of controlling or designing special grain boundaries, the impurity segregation, intergranular corrosion, and the resistance to carbide precipitation are remarkably improved^[10,11]. It has been reported that hydrogen can induce twinning to improve the deformability of TiAl based alloys^[20-22]. Furthermore, the mechanism of hydrogen-promoted $60^\circ\langle 111 \rangle$ and $180^\circ\langle 111 \rangle$ twinning is revealed and hydrogen-promoted $120^\circ\langle 111 \rangle$ twinning is found during hot deformation of a Ti-46Al-2V-1Cr-0.3Ni (at%) alloy^[23]. However, the mechanism of hydrogen-promoted $120^\circ\langle 111 \rangle$ twinning is still not clear, which makes it hard to conduct $120^\circ\langle 111 \rangle$ twin boundary design. Therefore, $120^\circ\langle 111 \rangle$ twin boundaries in γ phase of a TiAl based alloy during annealing treatment in hydrogen atmosphere was investigated in this research.

1 Experiment

Received date: September 25, 2018

Foundation item: National Natural Science Foundation of China (51275132, 51705199, 51372101); Shandong Provincial Natural Science Foundation, China (ZR2017BEE055); Distinguished Middle-Aged and Young Scientist Encouragement and Reward Foundation of Shandong Province (ZR2016EMB01); Taishan Scholar Engineering Special Funding (2016-2020)

Corresponding author: Zong Yingying, Ph. D., Professor, State Key Laboratory of Advanced Welding and Joining & School of Materials Science and Engineering, Harbin Institute of Technology, Harbin 150001, P. R. China, Tel: 0086-451-86416221, E-mail: hagongda@hit.edu.cn

Copyright © 2019, Northwest Institute for Nonferrous Metal Research. Published by Science Press. All rights reserved.

The experimental material was Ti-46Al-2V-1Cr-0.3Ni (at%) alloy fabricated by an alloy induction skull melting technique. Cylindrical billets with dimensions of $\Phi 37$ mm \times 50 mm were packed by 321 stainless steel and then two-step forged at the temperature of 1220 °C and speed of 0.8 mm/s, with a total engineering strain of 75%, and eventually the as-forged alloy was obtained. Samples with dimensions of 10 mm \times 8 mm \times 5 mm were obtained from the as-cast and as-forged alloys. Then, annealing treatment in hydrogen atmosphere test was conducted, and three samples were tested under each experiment condition, as shown in Table 1. Finally, microstructure of these samples was observed by an OLYMPUS GX71 optical microscope (OM), a Quanta 200FEG scanning electron microscope (SEM), an electron back scattered diffraction technique (EBSD) as an additional characterization technique in SEM, a Tecnai G²F30 transmission electron microscope (TEM), and a D/max-rB 12 kW X-ray diffraction (XRD) apparatus.

2 Results and Discussion

Fig.1 shows the OM, SEM microstructures and XRD pattern of the as-cast and as-forge Ti-46Al-2V-1Cr-0.3Ni alloys. As shown in Fig.1a and 1c, the as-cast alloy comprised coarse $\gamma+\alpha_2$ phase lamellar colonies with a mean size of approximately 870 μ m, a few fine γ -phase grains distributed along lamellar colony boundaries, and γ phase was dominant. In the as-forged alloy, γ phase (grey areas) was also dominant in the as-forged billet, with a volume fraction of 91.5%, and a little α_2 +B2 phase (white areas) could be observed, as shown in Fig.1b. Because γ phase was the main research object, α_2 and B2 phases were not indicated in the EBSD observations (see the white areas).

The grain orientation spread (GOS) in each grain is determined by calculating the average misorientation between all points sampled within the grain, and GOS maps can be used to determine recrystallization grains which typically have an orientation spread less than $1^\circ\sim 2^\circ$ ^[24]. Additionally, the critical GOS value (CGV) to determine recrystallization grains can be viewed as the end point of the first prominent peak^[25,26]. Fig.2 shows the GOS distribution maps of the samples C-I,

Table 1 Samples under different annealing treatment in hydrogen atmosphere

Samples	Status	Annealing treatment	H content/at%
C-I	As-cast	750 °C, 2 h, without hydrogen; furnace cooling	0
C-II	As-cast	750 °C, 2 h, with hydrogen pressure of 0.148 MPa; furnace cooling	0.8
F-I	As-forged	750 °C, 2 h, with hydrogen pressure of 0.117 MPa; furnace cooling	0.2
F-II	As-forged	750 °C, 2 h, with hydrogen pressure of 0.132 MPa; furnace cooling	0.4
F-III	As-forged	750 °C, 2 h, with hydrogen pressure of 0.136 MPa; furnace cooling	0.64
F-IV	As-forged	750 °C, 2 h, with hydrogen pressure of 0.148 MPa; furnace cooling	0.8

C-II, F-I, F-II, F-III and F-IV. CGVs of the samples C-I, C-II, F-I, F-II, F-III and F-IV were 0.93°, 1°, 1.13°, 1.3°, 0.9° and 0.8°, respectively, all of which were less than 2°. Consequently, their static recrystallization (SRX) fractions were 79%, 84.3%, 85.3%, 87.3%, 90.3% and 91.1%, respectively. Obviously, the SRX fraction increased due to hydrogen addition, and increased with increasing hydrogen content. Furthermore, many grains determined as SRX grains possessed $120^\circ\langle 111 \rangle$ twin boundaries. Note that $120^\circ\langle 111 \rangle$ meant the orientation relationship between the SRX grains and the parent grains was 120° around $\langle 111 \rangle$ direction.

Fig.3 shows the distribution maps of $120^\circ\langle 111 \rangle$ twin boundaries of the samples C-I, C-II, F-I and F-IV. Obviously, most of the SRX grain boundaries consisted of $120^\circ\langle 111 \rangle$ twin boundaries. As shown in the inset (a₁) of Fig.3, the SRX grains nucleated in the curved γ/α_2 interface (marked by dotted line) and grew into (marked by red arrows) an adjacent γ -phase lamella. The inset (a₂) of Fig.3 shows a TEM image of the as-cast alloy before hydrogenation. Obviously, curved γ/α_2 interfaces were common in the as-cast alloy, and meanwhile coherency strain generating dislocations could be also observed. Similarly, it could be observed that some SRX grains formed along grain boundaries and grew into the

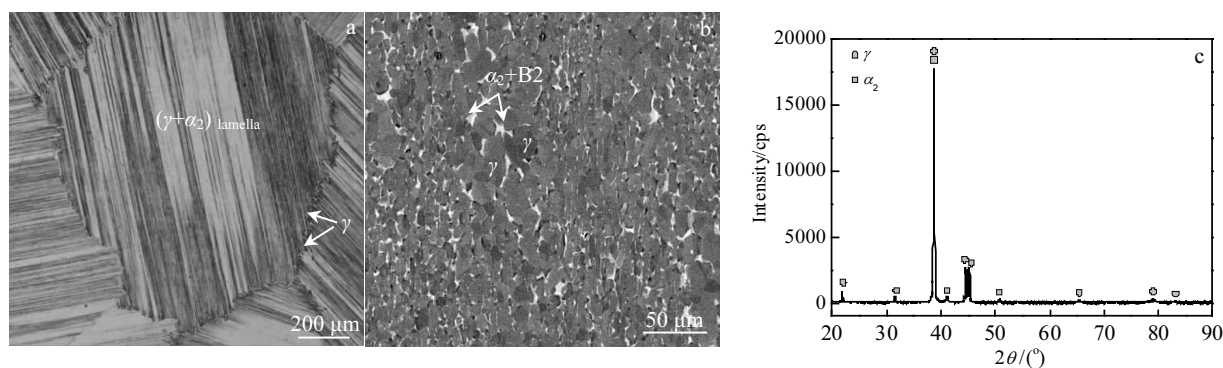


Fig.1 OM (a), SEM (b) microstructures and XRD pattern (c) of the as-cast (a, c) and as-forge (b) Ti-46Al-2V-1Cr-0.3Ni alloys

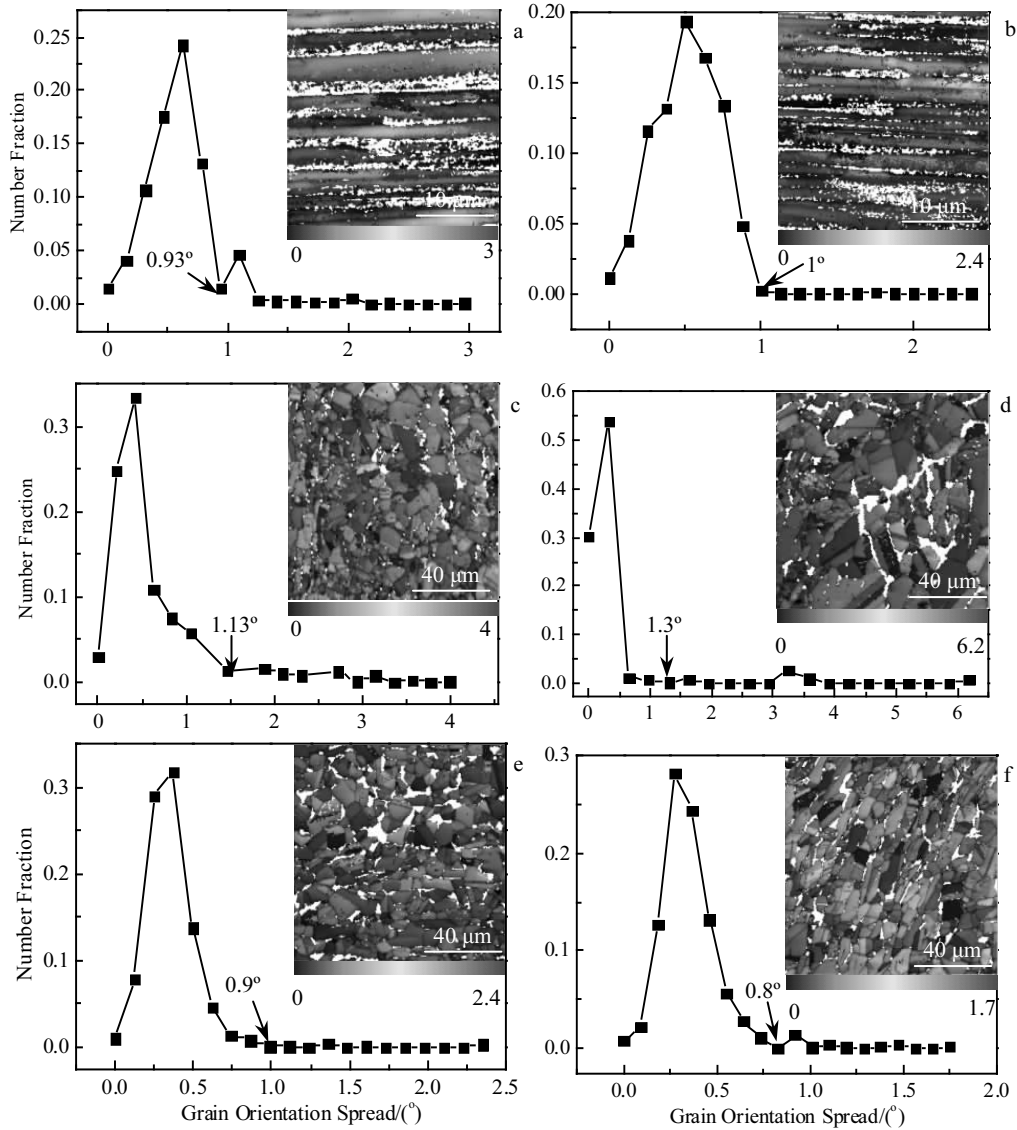


Fig.2 GOS distribution maps of the samples: (a) C-I, (b) C-II, (c) F-I, (d) F-II, (e) F-III, and (f) F-IV

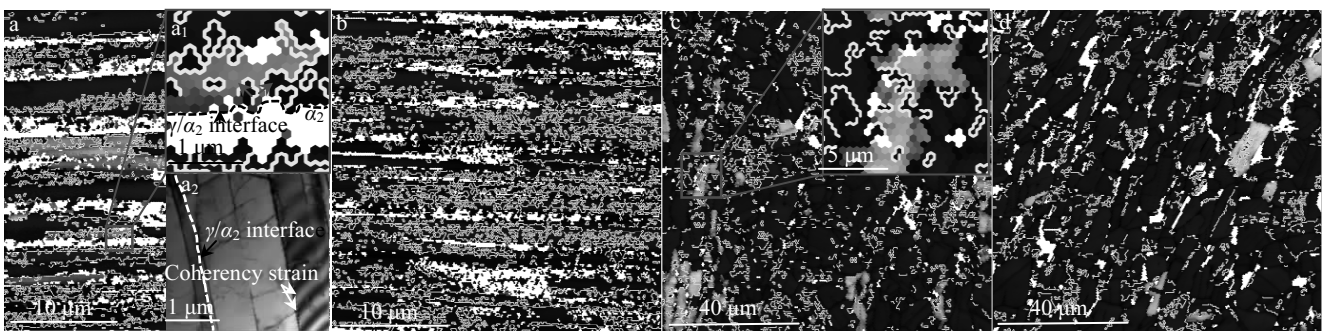


Fig.3 Distribution maps of 120°<111> twin boundaries of the samples: (a) C-I, (b) C-II, (c) F-I, and (d) F-IV (grains with blue color were determined as SRX grains, the yellow line meant 120°<111> twin boundaries and the inset (a₂) was a TEM image of the as-cast alloy before hydrogenation)

adjacent γ -phase grains in the as-forged alloy after hydrogenation, as shown in the inset of Fig.3c. For the as-cast alloys, the fraction of $120^\circ\langle 111 \rangle$ twin boundaries in the sample C-II was 81.9%, more than that (72.1%) in the sample C-I. Similarly, for the as-forged alloys, the fraction of $120^\circ\langle 111 \rangle$ twin boundaries increased with increasing hydrogen content. Fig.4 shows the dependence of $120^\circ\langle 111 \rangle$ twin boundary fractions on hydrogen content in the samples F-I, F-II, F-III and F-IV. The relationship between the the fraction of $120^\circ\langle 111 \rangle$ twin boundaries ($C_{120^\circ\langle 111 \rangle}$) and hydrogen content (C_H) could be described as:

$$C_{120^\circ\langle 111 \rangle} = 15.26C_H + 32.86 \quad (\%, \text{ for the as-forged alloy}) \quad (1)$$

Recrystallization is defined as the formation of a new grain structure by the formation and migration of high angle grain boundaries ($15^\circ\sim 180^\circ$) driven by the stored energy of deformation. Nevertheless, recrystallization can also be triggered by the stored strain due to residual quenching stresses, microstructural imperfections^[27,28], coherency strains due to lattice misfits during phase transformation, and high strain energy due to rapid growth of lamella^[29]. According to the phase diagrams of TiAl based alloys^[30,31], the recrystallization temperature of the present alloy is about 477 °C, and hence recrystallization can occur in both the unhydrogenated and hydrogenated alloys during annealing treatment. Therefore, many SRX grains were observed in the samples C-I and C-II after hydrogenation. It has been reported that hydrogen can promote recrystallization of the Ti-46Al-2V-1Cr alloy during the high-temperature deformation, which is partly attributed to hydrogen-increased element diffusion^[32,33]. That also partly contributed to the more SRX grains in the samples with hydrogen addition.

As shown in Fig.3, dominant $120^\circ\langle 111 \rangle$ twin boundaries were distributed in the SRX grains. It has been reported that the formation of $120^\circ\langle 111 \rangle$ twin boundaries was due to strain generated by the $\alpha_2 \rightarrow \gamma$ transformation^[34]. However, the formation of $120^\circ\langle 111 \rangle$ twin boundaries was also related to recrystallization. It is reported that recrystallization grains are preferentially oriented (i.e. recrystallization texture) according to the oriented nucleation

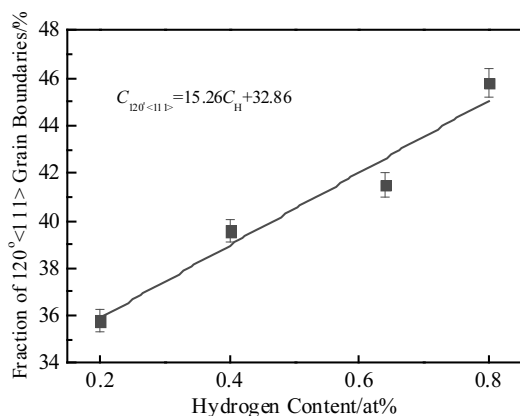


Fig.4 Dependence of $120^\circ\langle 111 \rangle$ twin boundary fractions on hydrogen content in the samples F-I, F-II, F-III and F-IV

and growth theories^[35,36]. It is generally agreed that a major driving force for recrystallization is the stored energy due to dislocations generated during deformation^[37]. Lee proposed strain energy release maximization model (SERMM) where the absolute maximum stress direction will become the direction of the minimum elastic modulus of recrystallization grains to reduce the stored energy^[38]. Note that SERMM is based on elastic anisotropy^[38,39]. The anisotropy indexes, A_G and A^U , can be given by^[40,41]

$$A_G = \frac{G_V - G_R}{G_V + G_R} \times 100\% \quad (2)$$

$$A^U = 5 \frac{G_V}{G_R} + \frac{B_V}{B_R} - 6 \quad (3)$$

where G and B are shear and bulk moduli, respectively, and the subscripts V and R denote the Voigt and Reuss approximations, respectively.

According to Eq.(2), and Eq.(3), the A_G and A^U of the unhydrogenated alloy were 8.965 and 0.914, respectively, which were consistent with the results by Chen et al.^[42]. According to SERMM, the formation of SRX grains can lead to the strain energy release maximization. However, numerous SRX grains possess $120^\circ\langle 111 \rangle$ twin boundaries whose interface energy is approximately 250 mJ/m², more than that of the $180^\circ\langle 111 \rangle$ twin boundaries^[43]. That means the formation of SRX grains with $120^\circ\langle 111 \rangle$ twin boundaries can not be completely explained by SERMM. Similarly, the recrystallization grains with $27^\circ\langle 110 \rangle$ grain boundaries can also not be explained by SERMM in a rolled V-4Cr-4Ti alloy, because SERMM is proposed according to the elastic anisotropy of steel which is opposite to the V-4Cr-4Ti alloy^[44]. The elastic anisotropy of the unhydrogenated alloy in this paper is lower than that of steel. Furthermore, it is reported that hydrogen can remarkably weaken elastic anisotropy of a TiAl alloy, with A_G and A^U decrease of 48% and 50%, respectively^[42]. Therefore, hydrogen-weakened elastic anisotropy led to more $120^\circ\langle 111 \rangle$ twin boundaries in the hydrogenated alloy, compared with the unhydrogenated alloy.

3 Conclusions

1) Hydrogen can promote γ -phase static recrystallization of the as-cast and as-forged Ti-46Al-2V-1Cr-0.3Ni alloy, and the extent of static recrystallization increases with increasing the hydrogen content. Many static recrystallization grains possess $120^\circ\langle 111 \rangle$ twin boundaries.

2) For the as-forged alloy, the relationship between the fraction of $120^\circ\langle 111 \rangle$ twin boundaries ($C_{120^\circ\langle 111 \rangle}$) and hydrogen content (C_H) can be described as $C_{120^\circ\langle 111 \rangle} = 15.26C_H + 32.86$ (%). Hydrogen-weakened elastic anisotropy leads to more $120^\circ\langle 111 \rangle$ twin boundaries.

References

- 1 Dimiduk D M. *Mater Sci Eng A*[J], 1999, 263: 281

- 2 Cao J, Liu J K, Song X G et al. *Mater Des*[J], 2014, 56: 115
- 3 Loria E A. *Intermetallics*[J], 2000, 8: 1339
- 4 Povarova K B, Antonova A V, Bannykh I O. *Metally*[J], 2003, 5: 61
- 5 Bumps E S, Kessler H D, Hansen M et al. *Metall Trans AIME*[J], 1952, 194: 609
- 6 Gleiter H. *Acta Metall*[J], 1969, 17: 1421
- 7 Mahajan S, Pande C S, Imam M A. *Acta Mater*[J], 1997, 45: 2633
- 8 Galizia P, Baldisserri C, Capiani C. *Mater Des*[J], 2016, 109: 19
- 9 Liu G, Xin R, Liu F et al. *Mater Des*[J], 2016, 107: 503
- 10 Katnagallu S S, Mandal S, Nagaraja A C. *Metall Mater Trans A* [J], 2015, 46a: 4740
- 11 Kobayashi S, Kobayashi R, Watanabe T. *Acta Mater*[J], 2016, 102: 397
- 12 Xia S, Zhou B X, Chen W J. *J Mater Sci*[J], 2008, 43: 2990
- 13 Watanabe T. *Res Mech*[J], 1984, 11: 47
- 14 Randle V. *Acta Mater*[J], 2004, 52: 4067
- 15 Xia S, Zhou B X, Chen W J. *Metall Mater Trans A*[J], 2009, 40a: 3016
- 16 Liu T G, Xia S, Li H et al. *Mater Lett*[J], 2014, 133: 97
- 17 Randle V. *Acta Mater*[J], 1999, 47: 4187
- 18 Watanabe T. *J Mater Sci*[J], 2011, 46: 4095
- 19 Masoumi M, Santos L P M, Bastos I N et al. *Mater Des*[J], 2016, 91: 90
- 20 Liu X W, Su Y Q, Luo L S et al. *Int J Hydrog Energ*[J], 2010, 35: 13 322
- 21 Zong Y Y, Wen D S, Liu Z Y et al. *Mater Lett*[J], 2015, 142: 23
- 22 Wen D S, Zong Y Y, Wang Y Q et al. *Mater Sci Eng A*[J], 2016, 656: 151
- 23 Wen D S, Shan D B, Wang S R et al. *Mater Sci Eng A*[J], 2018, 710: 374
- 24 Barrett C D, Imandoust A, Oppedal A L et al. *Acta Mater*[J], 2017, 128: 270
- 25 Dong S L, Chen R R, Guo J J et al. *Mater Des*[J], 2015, 84: 118
- 26 Zhang H B, Zhang K F, Zhou H P et al. *Mater Des*[J], 2015, 80: 51
- 27 Dey S R, Hazotte A, Bouzy E et al. *Acta Mater*[J], 2005, 53: 3783
- 28 Dey S R, Bouzy E, Hazotte A et al. *Acta Mater*[J], 2008, 56: 2051
- 29 Guyon J, Hazotte A, Wagner F et al. *Acta Mater*[J], 2016, 103(29): 672
- 30 Schwaighofer E, Clemens H, Mayer S et al. *Intermetallics*[J], 2014, 44: 128
- 31 Clemens H, Boeck B, Wallgram W et al. *Experimental Studies and Thermodynamic Simulations of Phase Transformations in Ti-(41-45)Al-4Nb-1Mo-0.1B Alloys*[M]. Warrendale: MRS, 2008: 217
- 32 Zong Y Y, Wen D S, Guo B et al. *Mater Lett*[J], 2015, 152: 196
- 33 Zong Y Y, Wen D S, Wang Y Q et al. *Mater Sci Eng A*[J], 2016, 656: 151
- 34 Yamaguchi M, Umakoshi Y. *Prog Mater Sci*[J], 1990, 34: 1
- 35 Burgers W G, Louwse P C. *Manage Healthcare*[J], 1931, 67: 605
- 36 Barrett C S. *Transaction AIME*[J], 1940, 137: 128
- 37 Dong N L. *Int J Mech Sci*[J], 2000, 42(8): 1645
- 38 Nyung L D. *Scr Met Mater*[J], 1995, 32(10): 1689
- 39 Park Y B, Lee D N, Gottstein G. *Acta Mater*[J], 1998, 46(10): 1337
- 40 Ranganathan S I, Ostojastarzewski M. *Phys Rev Lett*[J], 2008, 101: 1
- 41 Chung D H, Buessem W R. *Anisotropy in Single Crystal Refractory Compounds*[M]. New York: Plenum, 1968: 165
- 42 Chen S, Liang C P, Gong H R. *Int J Hydrogen Energy*[J], 2012, 37(3): 2676
- 43 Kanani M, Hartmaier A, Janisch R. *Intermetallics*[J], 2014, 54(54): 154
- 44 Peng L X, Li X W, Fan Z J et al. *Mater Charact*[J], 2017, 126: 35

TiAl 基合金在置氢退火过程中 γ 相 $120^\circ\langle 111 \rangle$ 孪晶界形成机制研究

温道胜¹, 王守仁¹, 单德彬², 宗影影²

(1. 济南大学, 山东 济南 250022)

(2. 哈尔滨工业大学 先进焊接与连接国家重点实验室, 黑龙江 哈尔滨 150001)

摘要: 利用金相显微镜、扫描电镜、EBSD 技术、透射电镜和 X 射线衍射研究了铸态和锻态 Ti-46Al-2V-1Cr-0.3Ni 合金退火过程中氢对 γ 相 $120^\circ\langle 111 \rangle$ 孪晶界的影响规律。结果表明, 氢可以促进铸态和锻态合金 γ 相的静态再结晶, 并且再结晶程度随氢含量的增加而增大; 大量再结晶晶粒具有 $120^\circ\langle 111 \rangle$ 孪晶界, 并揭示了 $120^\circ\langle 111 \rangle$ 孪晶界含量与氢含量的关系。氢致 $120^\circ\langle 111 \rangle$ 孪晶界增多的原因是氢减弱了 γ 相的弹性各向异性。

关键词: TiAl 基合金; 退火热处理; 氢; 静态再结晶; $120^\circ\langle 111 \rangle$ 孪晶界

作者简介: 温道胜, 男, 1983 年生, 博士, 济南大学机械工程学院, 山东 济南 250022, E-mail: daoshenghit@163.com